AIAA 2002–0588

Numerical Investigation of Flow past a Prolate Spheroid

George S. Constantinescu
Center for Integrated Turbulence Simulations, Stanford University, Stanford, CA 94305

Hugo Pasinato
MAE Department, Arizona State University, Tempe, AZ 85287-6016

You-Qin Wang
University of Northern British Columbia, Prince George, British Columbia V2N 4Z9, Canada

Kyle D. Squires
MAE Department, Arizona State University, Tempe, AZ 85287-6016

Aerospace Sciences Meeting 2002
14–18 January 2002 / Reno, Nevada

Numerical Investigation of Flow past a Prolate Spheroid

George S. Constantinescu
Center for Integrated Turbulence Simulations, Stanford University, Stanford, CA 94305
Hugo Pasinato
MAE Department, Arizona State University, Tempe, AZ 85287-6016
You-Qin Wang
University of Northern British Columbia, Prince George, British Columbia V2N 4Z9, Canada
Kyle D. Squires*
MAE Department, Arizona State University, Tempe, AZ 85287-6016

The flow field around a 6:1 prolate spheroid at angle of attack is predicted using solutions of the Reynolds-averaged Navier-Stokes equations and Detached-Eddy Simulation. The calculations were performed for the same conditions as measured by Chesnakas and Simpson[1] and Wetzel *et al.*[19] The Reynolds number is 4.2×10^6, the flow is tripped at $x/L = 0.2$, and the angle of attack α is varied from 10 to 20 degrees. RANS calculations are performed using the Spalart-Allmaras one-equation model[10] (referred to as 'S-A' throughout). The influence of corrections to the S-A model accounting for streamline curvature and a non-linear constitutive relation are also considered. DES predictions are evaluated against the experimental measurements, RANS results, as well as calculations performed without an explicit turbulence model. In general, flow field predictions of the mean properties from the RANS and DES are similar. While initiated further along the spheroid compared to experimental measurements, predictions of primary and secondary separation agree reasonably well with measured values. Solutions of the flow obtained without any explicit turbulence model produce substantial errors in skin friction and pressure distributions.

Introduction

FLOW separation in three-dimensional configurations poses one of the interesting and challenging problems encountered in fluid mechanics. Boundary layer detachment is almost always accompanied by undesirable effects such as loss of lift, increases in drag, amplification of unsteady fluctuations in the pressure field, etc. Prediction of three-dimensional separated flows over maneuvering bodies forms the over-arching interest of the present investigations. The particular focus of this contribution is on the flow field that develops around a prolate spheroid at a fixed angle of attack.

Three-dimensional separations strongly challenge analysis and predictive models. Work on two-dimensional separations, by comparison, is more developed and has provided detailed descriptions of the conditions influencing many separated flows, e.g., effects of adverse pressure gradient, flow reversal, etc. In three-dimensional flows, separation characteristics can be sensitive to the body geometry and angle of attack, Reynolds number, etc. Flow reversal and vanishing of the shear stress are two well-known effects that may not accompany three-dimensional separations.

Aside from the complex topology of the flow patterns, three-dimensional separated flows pose strong challenges to models. In this work, numerical simulation is used to predict the flow around a 6:1 prolate spheroid at angle of attack. Recent calculations of the flow over a prolate spheroid include the Reynolds-averaged calculations of Tsai and Whitney[18] and Rhee and Hino and Large Eddy Simulations of Hedin *et al.*[5] Reynolds-averaged methods possess the advantage of being computationally efficient, though application of RANS models to flows with massive separation appears beyond the reach of conventional RANS closures.[12] LES is a powerful approach since it resolves, rather than models, the large energy-containing scales of motion that are responsible for the bulk of momentum transport. Application to high Reynolds number flows requires additional empiricism in treatment of the wall layer, an active and unresolved area of current research.

Detached Eddy Simulation (DES) is a hybrid approach which attempts to capitalize on the often adequate performance of RANS models in predicting boundary layer growth and separation, and to use LES away from solid surfaces to model the typically geometry-dependent and unsteady scales of motion in

*author to whom correspondence should be addressed

separated regions.[12,13] DES is well suited for prediction of massively separated flows and applications of the technique to a range of configurations have been favorable.[3,9,15,17] In massively separated flows, turbulence structure in the wake develops rapidly through amplification of instabilities that overwhelm whatever structural content (or lack of) is transported from upstream in the boundary layers. The lack of eddy content in the attached boundary layers that are treated using a RANS closure has not resulted in substantial errors in predicting flows experiencing massive separation.

The flow over a prolate spheroid challenges DES because it is not massively separated, characterized by a region of chaotic, recirculating fluctuations, etc. The advantage of DES in providing more realistic descriptions of three-dimensional and unsteady motions in the wake of a massively separated flow is less clear cut in the spheroid since the structures in the separated region may not even possess any region of reversed flow, for example. In addition, experiments show that the an important element of the structure on the lee side of the spheroid are coherent streamwise vortices, structures that are relatively stable compared to the eddies that dominate the wakes of cylinder, spheres, or the region behind an airfoil at high angle of attack.

The main goal of this study is to apply DES to prediction of the flow around a prolate spheroid. The computations are assessed not only via comparison to measurements, but also using RANS predictions and solution of the flow field without any explicit turbulence model. The standard S-A model forms the backbone for the RANS solutions in this study (as well as comprising the base model in DES). Enhancements to the RANS model are investigated, specifically corrections for streamline curvature[11] and the use of a non-linear constitutive relation.[12] The interest is to gauge the level of improvement possible in RANS when an existing model for which there is a substantial experience base is augmented in an attempt to account for particular effects. In the longer-term, such enhancements could be easily incorporated into a DES formulation.

Presented in the next section is an overview of the numerical approach. The Spalart-Allmaras one-equation model is summarized along with the simple modification require to obtain the DES formulation. Details of the numerical method, grids, etc., are then summarized. A representative sampling of some of the statistical features of the flow are presented and finally a summary of the study.

Overview and Approach

Spalart-Allmaras Model

In the S-A RANS model, a transport equation is used to compute a working variable used to form the turbulent eddy viscosity,

$$\begin{aligned}\frac{D\widetilde{\nu}}{Dt} &= c_{b1}[1-f_{t2}]\widetilde{S}\,\widetilde{\nu} - \left[c_{w1}f_w - \frac{c_{b1}}{\kappa^2}f_{t2}\right]\left[\frac{\widetilde{\nu}}{d}\right]^2 \\ &+ \frac{1}{\sigma}\left[\nabla\cdot((\nu+\widetilde{\nu})\nabla\widetilde{\nu}) + c_{b2}\left(\nabla\widetilde{\nu}\right)^2\right], \\ &+ f_{t1}\,\Delta U^2\,, \end{aligned} \tag{1}$$

where $\widetilde{\nu}$ is the working variable. The eddy viscosity ν_t is obtained from,

$$\nu_t = \widetilde{\nu}\,f_{v1}, \qquad f_{v1} = \frac{\chi^3}{\chi^3+c_{v1}^3}, \qquad \chi \equiv \frac{\widetilde{\nu}}{\nu}, \tag{2}$$

where ν is the molecular viscosity. The production term is expressed as,

$$\widetilde{S} \equiv S + \frac{\widetilde{\nu}}{\kappa^2 d^2}f_{v2}, \tag{3}$$

$$f_{v2} = 1 - \frac{\chi}{1+\chi f_{v1}} \tag{4}$$

where S is the magnitude of the vorticity. The function f_w is given by,

$$\begin{aligned} f_w &= g\left[\frac{1+c_{w3}^6}{g^6+c_{w3}^6}\right]^{1/6} \\ g &= r + c_{w2}\,(r^6-r), \qquad r \equiv \frac{\widetilde{\nu}}{\widetilde{S}\kappa^2 d^2}\,. \end{aligned} \tag{5}$$

The function f_{t2} is defined as,

$$f_{t2} = c_{t3}\exp(-c_{t4}\chi^2)\,. \tag{6}$$

The trip function f_{t1} is specified in terms of the distance d_t from the field point to the trip, the wall vorticity ω_t at the trip, and ΔU which is the difference between the velocity at the field point and that at the trip,

$$f_{t1} = c_{t1}g_t\exp\left(-c_{t2}\frac{\omega_t^2}{\Delta U^2}\left[d^2+g_t^2d_t^2\right]\right), \tag{7}$$

where $g_t = \min(0.1, \Delta U/\omega_t\Delta x)$ and Δx is the grid spacing along the wall at the trip. The wall boundary condition is $\widetilde{\nu}=0$ and the constants are $c_{b1}=0.1355$, $\sigma=2/3$, $c_{b2}=0.622$, $\kappa=0.41$, $c_{w1}=c_{b1}/\kappa^2+(1+c_{b2})/\sigma$, $c_{w2}=0.3$, $c_{w3}=2$, $c_{v1}=7.1$, $c_{v2}=5$, $c_{t1}=1$, $c_{t2}=2$, $c_{t3}=1.1$, and $c_{t4}=2$.

Detached-Eddy Simulation

The DES formulation is based on a modification to the Spalart-Allmaras RANS model[10] such that the model reduces to its RANS formulation near solid surfaces and to a subgrid model away from the wall.[12] The basis is to attempt to take advantage of the usually adequate performance of RANS models in the thin shear layers where these models are calibrated and the power of LES for resolution of geometry-dependent

and three-dimensional eddies. The DES formulation is obtained by replacing in the S-A model the distance to the nearest wall, d, by $\widetilde{d}$, where $\widetilde{d}$ is defined as,

$$\widetilde{d} \equiv \min(d, C_{DES}\Delta)\,, \tag{8}$$

with

$$\Delta \equiv \max(\Delta x, \Delta y, \Delta z)\,. \tag{9}$$

where Δx, Δy, and Δz are the grid spacings. In "natural" applications of DES, the wall-parallel grid spacings (e.g., streamwise and spanwise) are at least on the order of the boundary layer thickness and the S-A RANS model is retained throughout the boundary layer, i.e., $\widetilde{d} = d$. Consequently, prediction of boundary layer separation is determined in the 'RANS mode' of DES. Away from solid boundaries, the closure is a one-equation model for the SGS eddy viscosity. When the production and destruction terms of the model are balanced, the length scale $\widetilde{d} = C_{DES}\Delta$ in the LES region yields a Smagorinsky eddy viscosity $\widetilde{\nu} \propto S\Delta^2$. Analogous to classical LES, the role of Δ is to allow the energy cascade down to the grid size; roughly, it makes the pseudo-Kolmogorov length scale, based on the eddy viscosity, proportional to the grid spacing. The additional model constant $C_{DES} = 0.65$ was set in homogeneous turbulence[9] and used without modification in this work.

Numerical Approach

Turbulent flow around the spheroid has been calculated through numerical solution of both the incompressible and compressible Navier-Stokes equations. The incompressible flow is computed using a fractional step method in which the governing equations are transformed to generalized curvilinear coordinates with the primitive velocities and pressure retained as the dependent variables. The base numerical method was previously employed by Constantinescu and Patel[2] for computation of steady flows. Extension to time-accurate calculations was performed using a double-time stepping algorithm as described in Johnson.[7] The numerical method is fully implicit with the momentum and turbulence transport equations discretized using fifth-order accurate upwind differences for the convective terms. All other operators are calculated using second-order central differences. The overall discretization scheme is second-order accurate in space, including at the boundaries.

As mentioned previously, one of the overall goals of this research is the development of accurate predictive methods for three-dimensional separated flows over maneuvering geometries. To this end, a compressible Navier-Stokes solver – Cobalt – capable of computing geometries undergoing rigid-body motion has been used to predict the static flow over the spheroid. The numerical approach in Cobalt is based on a finite-volume approach and is second-order accurate in space and time.[14] The method is point-implicit, enabling

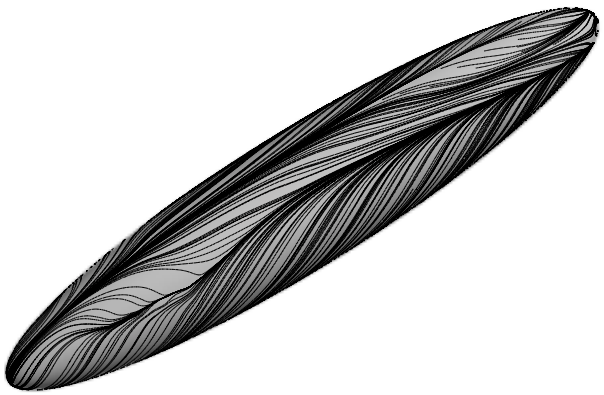

Fig. 1 Oil visualization, $\alpha = 20°$. Flow is tripped at $x/L = 0.2$.

CFL numbers as large as 10^6 for steady-state computations.[16] Computations are performed in parallel using the Message Passing Interface.

Grids for the spheroid were generated using the control technique of Hsu and Lee.[6] Using this approach it is possible to control grid density and enable a reasonably efficient distribution of points in the wake region. The grids are single block, calculations were carried out on a series of meshes ranging in grid sizes from 100 to 125 points along the body ("x"), 75 to 125 points in the azimuth, and 125 to 140 points normal to the spheroid. The outer boundary shape was elliptic, somewhat similar to the profile of the spheroid surface and extended 10 minor axes in front of the spheroid and 12 minor axes in the downstream direction. The first wall-normal grid point was within one viscous unit of the surface.

The inflow eddy viscosity was set to zero, with the trip terms applied on the surface of the spheroid at $x/L = 0.2$. For the incompressible flow, the velocity components and turbulent viscosity at the downstream boundary are obtained using second-order extrapolation from the interior of the domain. No-slip conditions on the spheroid surface are imposed. The pressure boundary condition on the sphere and at the upstream and downstream boundaries are obtained from the surface-normal momentum equation. Periodic boundary conditions are imposed on all variables in the azimuthal direction. On the polar axes, $(\theta = 0, \pi)$, the dependent variables are obtained by averaging over the azimuth a second-order accurate extrapolation of these variables. The timestep for most calculations was 0.01 (made dimensionless using the minor axis of the spheroid and freestream velocity).

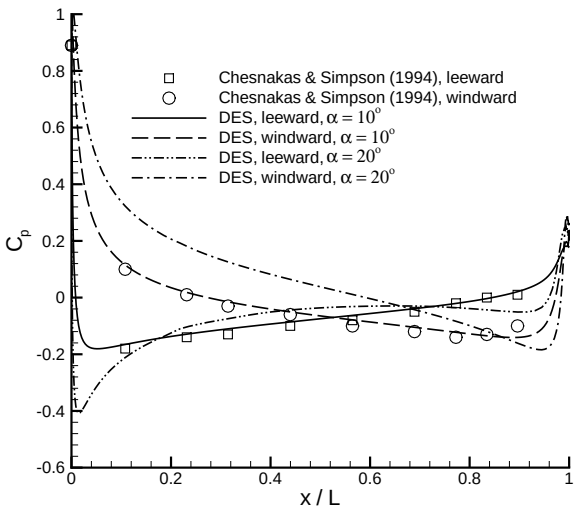

Fig. 2 Axial pressure distribution along windward and leeward surfaces for $\alpha = 10°$ and $20°$. Profiles taken along the symmetry plane.

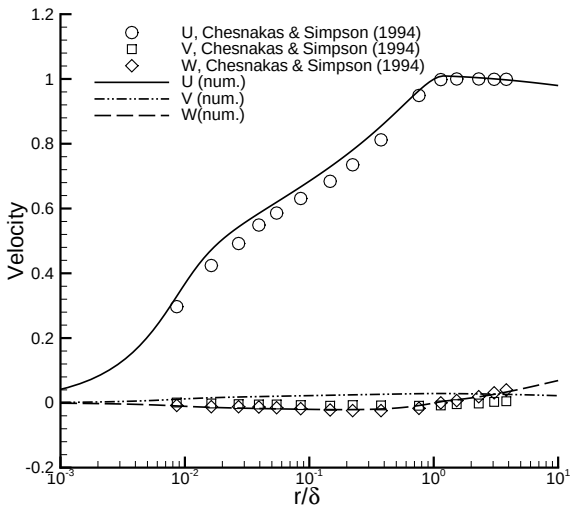

Fig. 3 Mean velocity profile for flow at $\alpha = 20°$. Profile at $x/L = 0.60$ and $\phi = 90°$.

Results

A representative example of some of the flow features around the spheroid is illustrated in Figure 1. The figure shows oil surface flow visualization for the S-A RANS prediction at 20° angle of attack. As in the experiments,[1,19] the boundary layer in the numerical solution is tripped at $x/L = 0.2$. On the windward side of the body an attached three-dimensional boundary layer is formed. As the flow passes along the body, boundary layer separation occurs on the lee side, corresponding to the convergence of the surface flows in Figure 1. The shed vorticity rolls up into a pair of longitudinal vortices. These vortices can induce a secondary separation that is predicted in the aft region in the configuration shown in Figure 1.

The pressure coefficient in the symmetry plane from DES predictions of the flow at 10° and 20° angle of attack are shown in Figure 2. Measurements of the distribution at 10° angle of attack are available from Chesnakas and Simpson.[1] As can be observed in the figure, the agreement between simulation and experiment for $\alpha = 10°$ is mostly good, especially on the leeward side. Along the windward side in the aft region there is some discrepancy, one contributor could be the presence of the support sting used in the experiments and not included in the computations. Compared to the distribution at $\alpha = 10°$, the profiles from the DES at 20° angle of attack exhibit greater streamwise variation, corresponding to the stronger acceleration of the flow over most of the spheroid on the windward side and greater deceleration over most of the lee side of the body.

The mean velocity components from the DES prediction of the flow at 20° angle of attack is shown in

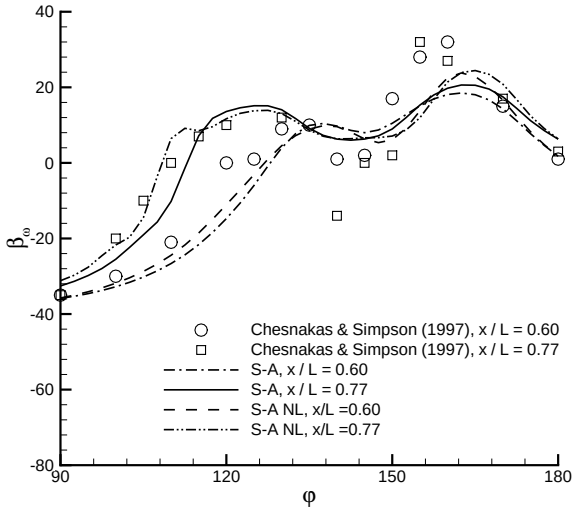

Fig. 4 Azimuthal distribution of wall-flow turning angle, freestream at $\alpha = 20°$ angle of attack.

Figure 3. The profiles shown are at an axial position $x/L = 0.6$ and azimuthal angle of $\phi = 90°$. The plot has been made dimensionless using the local boundary layer thickness and freestream speed. Overall, the agreement with measurements is adequate. The near-wall flow is resolved, with the simulation yielding a logarithmic region as measured in the experiments.[1] Agreement in the y and z component velocities is fair. Though not shown here, velocity hodographs yield about the same level of agreement between simulation and experiment as observed in the mean flow in Figure 3.

The wall-flow turning angle, β_w, is shown in Figure 4. The angle β_w measure the direction of the

flow at the wall relative to the streamwise direction. Predictions using the standard S-A model are plotted along with results obtained using a non-linear constitutive relation. The non-linear model is that proposed by Spalart[13] in which the Reynolds stress from the linear model (S-A, in this case) is related to the non-linear stress via,

$$\tau_{ij} = \overline{\tau}_{ij} - c_{nl}\left[O_{ik}\overline{\tau}_{jk} + O_{jk}\overline{\tau}_{ik}\right], \qquad (10)$$

where

$$O_{ik} = \frac{\partial_k U_i - \partial_i U_k}{\sqrt{\partial_n U_m - \partial_m U_n}}. \qquad (11)$$

is the normalized rotation tensor. As described in Spalart,[12] the constant $c_{nl} = 0.3$ was calibrated in the outer region of a simple boundary layer by requiring a fair level of anisotropy. Applications to prediction of the fully developed flow in a square duct were positive, with secondary flows predicted and skin friction estimations closer to measurements[12] than those obtained using the linear model.

The solutions and measurements shown in Figure 4 are for the flow at 20° angle attack and at axial positions $x/L = 0.6$ and $x/L = 0.77$. The calculations closing the stress using (10) are denoted 'S-A NL' in the figure. Note also that the region plotted corresponds to $90 \leq \phi \leq 180$ degrees. For $x/L = 0.6$, there is not a significant difference in predictions of the turning angle for the two models. In general, there is a lag in the predicted turning compared to the measurements for ϕ less than about 135°. The strong variation in β_w measured in the vicinity of 150° coincides with the positions of the primary and secondary separations (c.f., Figure 7). Figure 4 shows the azimuthal variation is not as pronounced in the simulations, using either model, Some differences emerge in predictions obtained using the two models at $x/L = 0.77$. The closure using the non-linear constitutive relation (10) exhibits less lag compared to the experimental measurements as found using the standard S-A model. The shift toward lower ϕ in the minima in β_w at $x/L = 0.77$ compared to $x/L = 0.6$ seems consistent with the measurements, though Figure 4 shows greater scatter in β_w measurements at $x/L = 0.77$.

Skin friction and pressure coefficients are shown in Figure 5 and Figure 6, respectively, for $\alpha = 20°$ and at an axial position $x/L = 0.77$. For this angle of attack and streamwise station measurements show the existence of both a primary and secondary separation on the spheroid. In addition to S-A results using the standard (linear) model, the non-linear relation (10), and DES, RANS predictions obtained from the S-A model with an explicit correction for rotation/curvature effects[11] are included (labeled S-A RC in the figures) together with simulations performed without any explicit turbulence model. The runs without a turbulence model are denoted as MILES (Monotone Integrated Large Eddy Simulation) to provide a link with

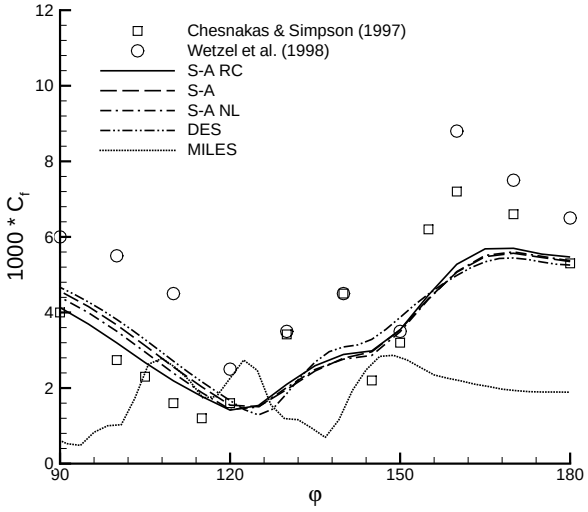

Fig. 5 Azimuthal distribution of skin friction coefficient at $x/L = 0.77$, flow at 20° angle of attack.

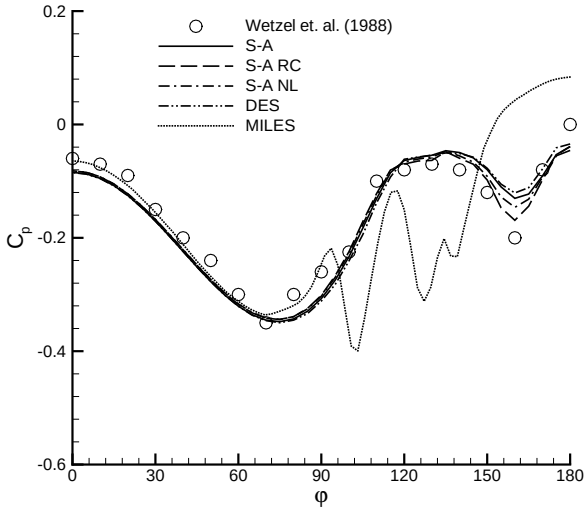

Fig. 6 Azimuthal distribution of the pressure coefficient at $x/L = 0.77$, flow at $\alpha = 20°$ angle of attack.

relevant literature, although no detailed investigations were undertaken to evaluate the numerical dissipation in the current calculations and its role as an SGS model, and the numerical schemes are not monotone in a strict sense (see Fureby and Grinstein[4] for a discussion of the MILES approach).

Two sets of skin friction measurements are shown in Figure 5. With the exception of the MILES prediction, the general trend of all the predictions is similar, following the data, but less peak-to-peak variation. The minima in C_f near $\phi \approx 150°$, for example, is one approach used to identify the separation location. The C_f distributions from all of the simulations show an inflection point in that vicinity, but without a clear sec-

ondary minima, indicative of a weaker shed structure in the calculations as compared to the experiments. Based on the skin friction, there is relatively little basis to distinguish the various models in terms of accuracy considerations, though the DES result shows a slightly lower global minimum around $\phi \approx 125°$ and perhaps greater peak-to-peak variation compared to the RANS model results. The MILES predictions of the skin friction are poor, providing an illustration of the importance of accurately modeling the boundary layer. On the windward side at $\phi = 0$, the skin friction prediction in the MILES is low, consistent with the fact that for the Reynolds number under consideration, it is not feasible to directly resolve boundary layer turbulence and MILES predicts an effectively laminar boundary layer. The MILES boundary layer then separates substantially earlier than in calculations performed with an explicit turbulence model.

Pressure coefficients shown in Figure 6 show similar effects as observed in the skin friction. The signature of the shed structures via the second minima in C_p is weaker in the calculations as compared to the experiments. The S-A calculation including the rotation/curvature correction is closest to the experimental measurement of the second minima, slightly superior to the DES result. Analogous to the skin friction, the MILES prediction of the pressure distribution differs substantially from both the experimental measurements and calculations performed using an explicit turbulence model.

The DES prediction of the primary and secondary separation lines is compared to measured values for $\alpha = 20°$ in Figure 7. Various experimental techniques have been employed to deduce separation locations. The figure shows some discrepancy in the position of the separation line prior to $x/L \approx 0.3$, but with generally good agreement among the different techniques in determination of the separation line further along the body. In general, the DES predictions of the onset of both the primary and secondary separations is delayed relative to that from the experiments, e.g., the primary separation is initiated slightly downstream of $x/L \approx= 0.4$. Considering the difficulty in unambiguosly identifying the onset of separation in three-dimensional flows, the agreement in the separation lines from DES and experiments seems mostly adequate.

Summary

The three-dimensional separated flow over a prolate spheroid has been predicted using RANS and DES. Simulation results were compared both to experimental measurements as well as to calculations in which an explicit turbulence model was not included.

Variations of the Spalart-Allmaras one-equation model were employed in the RANS. A non-linear constitutive relation was applied and shows some differences in prediction of quantities such as the wall flow turning angle. Prediction of azimuthal variations of the skin friction and pressure coefficient using the non-linear model showed relatively small differences compared to the standard S-A model. A stronger effect on the pressure variation was observed in calculations that incorporated the rotation/curvature correction to S-A.[11] While improving prediction of the signature of the longitudinal vortex on the mean pressure on the surface, it is noteworthy that in other regions the effect of the rotation/curvature correction did not interfere with already adequate predictions.

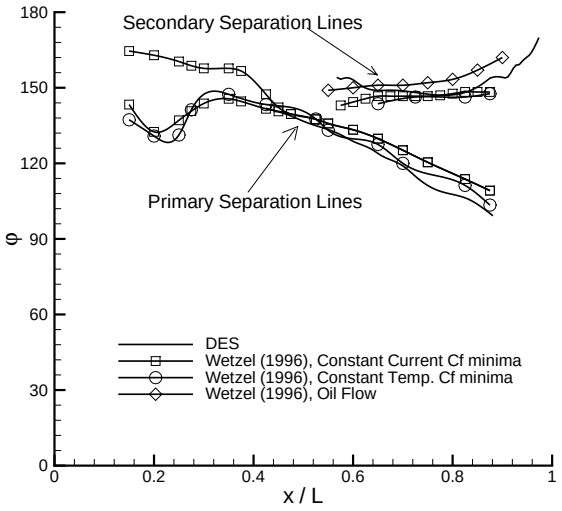

Fig. 7 Primary and secondary separation line predictions from DES compared to various indicators from experiments, $\alpha = 20°$

In general, for the angles of attack considered and the grid resolutions employed to date, there was not substantial differences in predictions of the mean quantities obtained using RANS and DES. Three-dimensional separated flows over the spheroid at low angles of attack are not characterized by overwhelming new instabilities as the boundary layer detaches from the surface. It remains to be determined the degree to which DES predictions can be altered by incorporating effects such as corrections for streamline curvature, for example, as well substantial refinement of the mesh in the LES region.

Acknowledgments

The authors gratefully acknowledge the support of the Office of Naval Research (Grant Numbers N00014-96-1-1251, N00014-97-1-0238, and N00014-99-1-0922, Program Officers: Dr. L. P. Purtell and Dr. C. Wark). The authors are also grateful for the insight and many useful comments from Dr. P. R. Spalart.

References

[1]Chesnakas, C.J. and Simpson, R.L., 1997, "Detailed investigation of the three-dimensional separation about a 6:1 prolate

spheroid", *AIAA Journal*, **35**(6), pp. 990-999.

[2]Constantinescu, G.S. and Patel, V.C., 1998, "A Numerical Model for Simulation of Pump-Intake Flow and Vortices," *Journal of Hydraulic Engineering*, **124**(2), pp. 123-134.

[3]Constantinescu, G.S. and Squires, K.D., 2000, "LES and DES investigations of turbulent flow over a sphere", *AIAA Paper 2000-0540*.

[4]Fureby, C. and Grinstein, F.F., "Monotonically integrated large eddy simulation of free shear flows", *AIAA J.*, **37**, pp. 544-556, 1999.

[5]Hedin, P.-O., Berglund, M., Alin, N. and Fureby, C., 2001, "Large eddy simulation of the flow around an inclined prolate spheroid", *AIAA Paper 20001-1035*.

[6]Hsu, K. and Lee, S.L., 1991, "A numerical technique for two-dimensional grid generation with grid control at all of the boundaries", *J. Computational Physics*, **11**, pp. 451-469.

[7]Johnson, T.A. and Patel, V.C., 1999, "Flow Past a Sphere up to a Reynolds Number of 300," *J. Fluid Mech.*, **378(1)**, pp. 19-70.

[8]Rhee, S.H. and Hino, T., 2000, "Computational investigation of 3D turbulent flow separation around a spheroid using an unstructured grid method", *J. Soc. Naval Architects of Japan*, **188**, pp. 1-9.

[9]Shur, M., Spalart, P. R., Strelets, M., and Travin, A, 1999, "Detached-Eddy Simulation of an Airfoil at High Angle of Attack", 4th Int. Symp. Eng. Turb. Modelling and Measurements, Corsica, May 24-26, 1999.

[10]Spalart, P.R. and Allmaras, S.R., 1994, "A One-Equation Turbulence Model for Aerodynamic Flows," *La Recherche Aerospatiale* **1**, pp. 5-21.

[11]Spalart, P.R. and Shur, M., 1997, "On the sensitization of simple turbulence models to rotation and curvature", *Aerosp. Sc. and Techn.*, **1**(5), pp. 297-302.

[12]Spalart, P.R. (2000), "Strategies for Turbulence Modeling and Simulations", *International Journal of Heat and Fluid Flow*, **21**, p. 252-263.

[13]Spalart, P.R., Jou, W.H., Strelets, M. and Allmaras, S.R., 1997, "Comments on the Feasibility of LES for Wings, and on a Hybrid RANS/LES Approach,", *First AFOSR International Conference on DNS/LES*, Ruston, Louisiana, USA.

[14]Strang, W.Z., Tomaro, R.F., Grismer, M.J., 1999, "The Defining Methods of Cobalt_{60}: a Parallel, Implicit, Unstructured Euler/Navier-Stokes Flow Solver", *AIAA 99-0786*, January 1999.

[15]Strelets, M., 2001, "Detached Eddy Simulation of Massively Separated Flows", *AIAA Paper 01-0879*.

[16]Tomaro, R.F., Strang, W.Z., and Sankar, L.N., 1997, "An Implicit Algorithm for Solving Time Dependent Flows on Unstructurd Grids", *AIAA 97-0333*, January 1997.

[17]Travin, A., Shur, M., Strelets, M. and Spalart, P.R. (2000), "Detached-eddy simulations past a circular cylinder", *Flow, Turbulence, and Combustion*, **63**, pp. 293-313.

[18]Tsai, C.-Y. and Whitney, A.K., 1999, "Numerical study of three-dimensional flow separation for a 6:1 ellipsoid", *AIAA Paper 99-0172*.

[19]Wetzel, T.G., Simpson, R.L. and Chesnakas, C.J., 1998, "Meaurement of three-dimensional crossflow separation", *AIAA Journal*, **36**(4), pp. 557-564.